



Contents lists available at ScienceDirect

Chemical Engineering Journal

journal homepage: www.elsevier.com/locate/cej

Immobilization and kinetic promotion of polysulfides by molybdenum carbide in lithium-sulfur batteries

Mengxue He^{a,b}, Xia Li^b, Weihan Li^b, Matthew Zheng^b, Jiajun Wang^a, Shaobo Ma^a, Yulin Ma^a, Geping Yin^a, Pengjian Zuo^{a,*}, Xueliang Sun^{b,*}

^a MIT Key Laboratory of Critical Materials Technology for New Energy Conversion and Storage, School of Chemistry and Chemical Engineering, Harbin Institute of Technology, Harbin 150001, China

^b Department of Mechanical and Materials Engineering, Western University, London, Ontario N6A 5B9, Canada

ARTICLE INFO

Keywords:

Kinetics promotion of LiPSs
Molybdenum carbide
Lithium sulfur battery
Separator modification

ABSTRACT

The shuttle effect of lithium polysulfides (LiPSs) intermediates is mainly responsible for the poor cycling stability of lithium sulfur (Li-S) batteries. Accelerating the reaction kinetics of the LiPSs conversion is proved to be effective in suppressing the migration of LiPSs. Herein, we propose an effective KB/Mo₂C-modified separator for enabling stable Li-S batteries. The Mo₂C shows both favorable anchoring capability and catalysis activity for LiPSs conversion due to its strong chemical affinity with LiPSs. The reaction kinetics of LiPSs reduction are facilitated on the Mo₂C surface, and the activation potential of lithium sulfide (Li₂S) oxidation is reduced. The battery using the modified separator shows high active material utilization and long-term cycling stability with a low decay rate of 0.076% per cycle up to 600 cycles at 1C. Moreover, when the sulfur loading increases to 6.5 mg cm⁻², a high areal capacity of 5.2 mAh cm⁻² can be maintained after 60 cycles with a capacity retention of 87%, demonstrating the feasibility for practical applications in Li-S batteries.

1. Introduction

Rechargeable batteries with long cycle life and high energy density are in urgent need with the advances in electric vehicles (EV) and portable electronic devices [1,2]. In comparison to the conventional lithium-ion batteries (LIBs), the Li-S battery is a promising candidate for the next generation of energy storage system owing to its high energy density of 2600 Wh kg⁻¹, low cost and nontoxicity of sulfur [3,4]. However, despite the remarkable merits, the practical application of Li-S batteries is hindered by serious capacity fading, which is mainly caused by the shuttling of LiPSs in the electrolyte and the chemical side reaction between the lithium anode and LiPSs [5,6]. In addition, the sluggish conversion kinetics of LiPSs further aggravate the shuttle effect and reduce the utilization of active materials [7].

In the past two decades, many approaches have been proposed to solve the abovementioned problems. The various carbon materials [8–11] are reported as sulfur host, enabling improved performance for Li-S batteries due to their good electronic conductivity and immobilization capability for sulfur species. However, the non-polar carbon materials suffer from a bottleneck in binding the polar LiPSs

intermediates. Consequently, some polar materials are introduced to create a polar condition to strengthen the affinity between the host materials and the LiPSs by heteroatom doping or surface modification of carbon materials. These materials not only show strong affinity with LiPSs but also exhibit positive effect on LiPSs conversion. Arava and co-workers find that the metallic current collectors such as Pt, Ni and Au can efficiently convert long-chain LiPSs to short-chain LiPSs as well as the inverse process [12]. Subsequently, more polar materials have been explored and have shown catalysis for LiPSs conversion, such as simple metal substance (Ir [13]), metal sulfides (CoS₂ [14]), metal oxides (Nb₂O₅ [15]), metal nitrides (TiN [16], Co₄N [17]), metal phosphides (MoP [18], CoP [19]) and metal carbides (TiC [20]). These reported polar materials demonstrate effective improvement for electrochemical cyclability owing to the accelerated reaction kinetics of LiPSs. However, the introduction of inert substances both increases the cost and reduces the energy density. Therefore, a catalyst with high conductivity and low cost will be high-efficiency to realize a smooth anchoring-conversion of LiPSs and improve the energy density. Molybdenum carbide (Mo₂C) which combines these two kinds of characteristics shows strong affinity with the LiPSs, effectively inhibiting the shuttle effect [21–25].

* Corresponding authors.

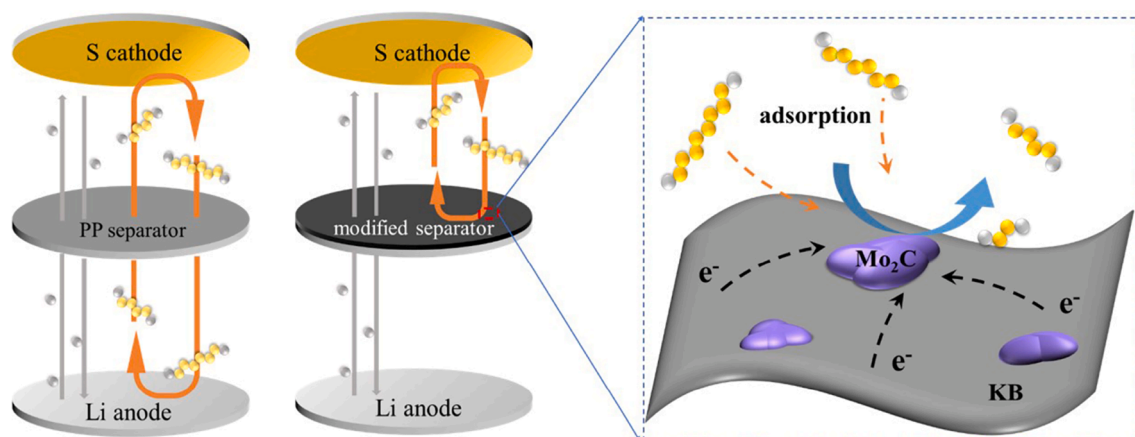
E-mail addresses: zuopj@hit.edu.cn (P. Zuo), xsun9@uwo.ca (X. Sun).

<https://doi.org/10.1016/j.cej.2021.128563>

Received 16 October 2020; Received in revised form 25 December 2020; Accepted 12 January 2021

Available online 18 January 2021

1385-8947/© 2021 Elsevier B.V. All rights reserved.



Scheme 1. Schematic diagram of a Li-S battery with KB/Mo₂C-modified separator.

However, the evolution of Mo₂C and LiPSs during the charge/discharge process is still unclear and needs to be further study.

In Li-S batteries, LiPSs will pass through the separator then react with the Li anode, resulting in poor cycling performance and low Coulombic efficiency. One efficient strategy to prevent this issue is to use a modified separator facing the sulfur cathode to prevent the permeation of LiPSs. Various carbon and polymer materials have been investigated as separator coatings to block the dissolved LiPSs migrating to the anode side in Li-S batteries [26,27]. Moreover, the conductive matrix in the coating as a current collector is helpful to reutilize the trapped polysulfides species in the following electrochemical reaction [28,29]. However, it should be noted that only employing non-polar carbon materials as coatings for a separator is not enough to build a strong chemical bonding between the separator and LiPSs. The incorporation of aforementioned polar materials and carbon materials together as coating materials for the separator is a straightforward strategy to trap LiPSs and catalyze their conversion.

Herein, we propose a multifunctional carbon/molybdenum carbide (KB/Mo₂C) decorated separator for Li-S batteries and explore the effect of the Mo₂C on the LiPSs conversion. As shown in Scheme 1, the KB/Mo₂C-modified separator as a barrier with active trapping sites for dissolved LiPSs is proposed to effectively alleviate the shuttle effect and improve the cycling performance of Li-S batteries. The KB/Mo₂C-modified separator has proved to be effective in hindering the diffusion of the LiPSs and further accelerating the conversion of LiPSs. In addition, the electron transfer between Mo and S, and the formation of stable C-Mo-S composite are confirmed by the synchrotron-based X-ray absorption spectroscopy (XAS) test. The Li-S battery with the KB/Mo₂C-modified separator demonstrates a high utilization of the active material and excellent rate performance with good cycling stability. A high areal capacity of 5.2 mAh cm⁻² was maintained after 60 cycles with a capacity retention of 87%, demonstrating its promise for practical applications of Li-S batteries.

2. Experimental section

2.1. Material synthesis

The KB/Mo₂C composite was prepared by carburization process at high temperature. 300 mg (NH₄)₆Mo₇O₂₄ was first dissolved in 18 mL ultrapure water and 2 mL ethanol. Then 800 mg commercial KB (Ketjen Black EC600JD) was added to the solution. The mixture was dried at 80 °C in vacuum for 12 h after being magnetically stirred for 6 h and put under ultrasonic treatment for 2 h. Finally, the mixture was heated at 800 °C for 3 h under Ar atmosphere with a heating rate of 5 °C min⁻¹. The KB/Mo₂C composite was obtained after cooling to ambient temperature.

2.2. Material characterization

The morphology observation was conducted within a Zeiss field-emission scanning electron microscope (Merlin Compact). The as-prepared products were characterized by an X-ray powder diffractometer with the range from 10° to 90° and Cu-Kα radiation source ($\lambda = 0.154$ nm). The content of sulfur or Mo₂C in the samples was confirmed by thermogravimetric analysis (TGA) (DSC, Netzsch STA449F3) in air with a heating rate of 10 °C min⁻¹. Transmission electron microscope (TEM) and high-resolution TEM (HRTEM) images was recorded by Tecnai G2 F30 microscope at 200 kV. UV/Vis absorption spectra of the electrolyte were collected using a Perkin Elmer LAMBDA 1050 spectrophotometer. The N₂ adsorption-desorption isotherms were recorded by 3H-2000PS1 gas adsorption analyzer. X-ray photoelectron spectra (XPS) were tested on a PHI model 5700 spectrometer. Ex-situ synchrotron-based X-ray absorption near edge structure (XANES) spectra was carried out at the Canadian Light Source (CLS). Sulfur K-edge was collected on the Soft X-ray Microcharacterization Beamline (SXRMB) by total electron yield (TEY) mode and the Mo K-edge spectra was collected on Hard X-ray Micro-Analysis (HXMA) beamline by fluorescent yield (FLY) mode. The tested separators were obtained by disassembling cells of different charge/discharge states in a glovebox under argon to avoid oxidation. Subsequently, the samples were transferred to different beamlines for testing.

2.3. Preparation of KB/Mo₂C-modified separators

The modified separator was prepared using a doctor blade coating process. In a typical procedure, the homogeneously slurry combined 90 wt% KB/Mo₂C with 10 wt% PVDF binder in 1-Methyl-2-pyrrolidinone (NMP) was coated onto the Celgard 2400 PP separator. The modified separator was cut into circular discs with diameter of 16 mm after dried at 50 °C for 24 h. The mass loading of the KB/Mo₂C on the separator was around 0.6 mg cm⁻².

2.4. Li-S cell assembly and measurements

Electrochemical performances were evaluated by 2025 type coin cells. The cathode slurry was prepared by mixing the DC/S, polyethylene oxide (PEO) binder and carbon black in weight ratio of 8: 8: 1 in deionized water. The well-mixed slurry was coated onto aluminum foil current collector and then dried at 50 °C for 12 h in a vacuum oven. The cathodes were punched into circular disks with diameter of 14 mm. The sulfur loading of the cathode used for the main electrochemical tests is around 1.2 mg cm⁻² and the high areal loading sulfur cathode (3.5 and 6.5 mg cm⁻²) was used to evaluate the effect of the areal density on performance. The lithium foil was used as the anode and the bare or

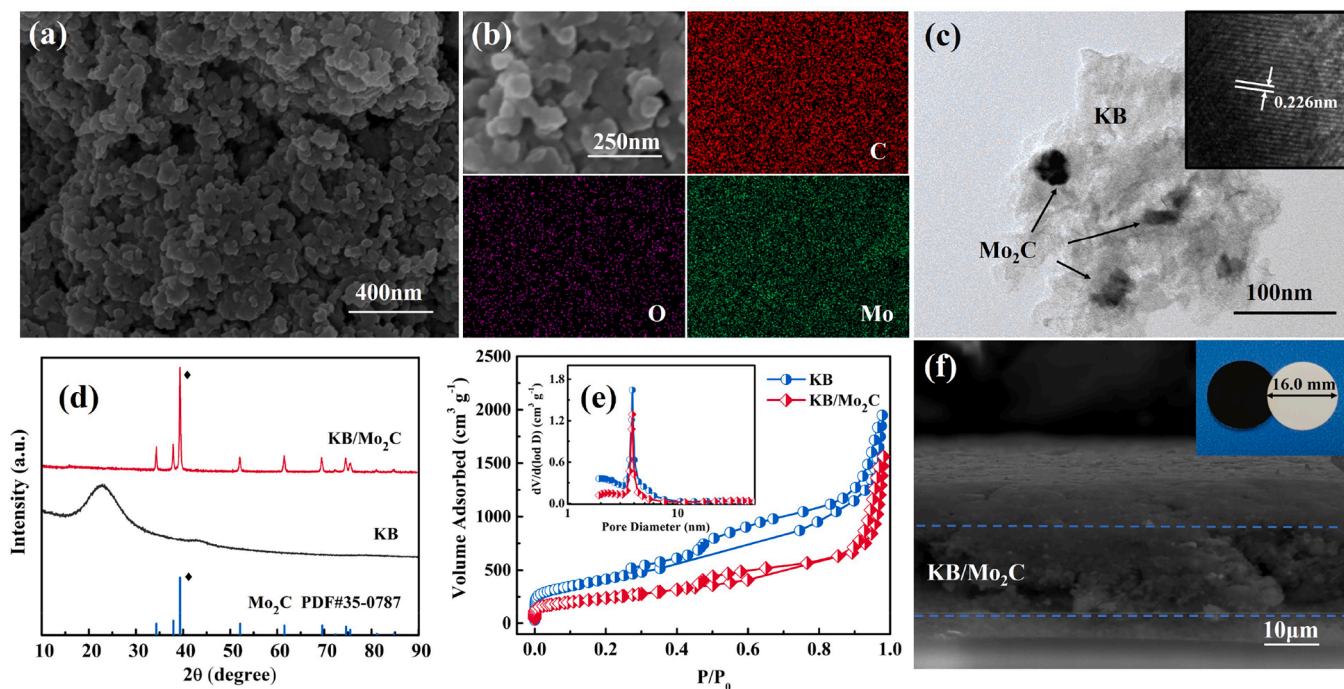


Fig. 1. (a) SEM image and (b) energy dispersive spectroscopic (EDS) elemental mappings of the KB/Mo₂C. (c) TEM and HRTEM (inset) images of the KB/Mo₂C. (d) XRD pattern of the composites. (e) N₂ adsorption-desorption analysis and corresponding pore size distributions (inset) of the materials. (f) Cross-section SEM image and digital picture of the KB/Mo₂C-modified separators.

modified separator was employed as separator. The functional coating side of the separator was facing to the cathode. The electrolyte used here was 1 M bis(trifluoromethane)sulfonamide lithium (LiTFSI, Sigma-Aldrich) and 0.4 M lithium nitrite (99.99% trace metals basis, Sigma-Aldrich) in a mixed solvent of DOL/DME (v/v = 1/1). The electrolyte without LiNO₃ was also prepared to compare the Coulombic efficiency. The cells were assembled in an argon-filled glove box with moisture and oxygen levels less than 1 ppm. Galvanostatic cycling was tested on Neware test system (BST-5 V 10 mA) between 1.7 and 2.6 V. The electrochemical impedance spectra (EIS) were conducted using an electrochemical workstation PARSTAT 2273 with a frequency range of 10 kHz to 10 mHz and an amplitude of 5 mV. Cyclic voltammetry curves were recorded using an AUTOLAB PGSTAT302N instrument at a scanning rate of 0.1 mV s⁻¹ between 1.5 and 3.0 V.

3. Results and discussion

The KB/Mo₂C material was prepared by heat-treating the mixture of KB (Fig. S1) and molybdenum precursors. The as-synthesized composite materials maintain the original morphology without evident agglomeration after annealing (Fig. 1a), and the distribution of Mo₂C in KB framework is homogenous as shown in the SEM-EDS elemental mapping (Fig. 1b). The oxygen element in the composite is mainly derived from the surface oxidation of the sample exposed in air [30]. The lattice fringes with a parallel distance of 0.226 nm can be well-distinguished in the HRTEM image (Fig. 1c, inset), which corresponds to the (101) planes of the Mo₂C crystal. The XRD pattern reveals the hexagonal phase structure for Mo₂C (PDF# 35-0787) (Fig. 1d). The mass loading of Mo₂C in KB/Mo₂C composite is approximate 24.8 wt% according to the TGA result (Fig. S2). The N₂ isotherm validates that pristine KB has specific surface area of 1497 m² g⁻¹ based on Brunauer-Emmett-Teller (BET) theory and an average pore size of 4 nm (Fig. 1e). The decreased specific surface area (870 m² g⁻¹) and pore volume for KB/Mo₂C are mainly caused by the blocking of the channel structure during the preparation process of Mo₂C nanoparticles. The KB/Mo₂C composite is coated on the surface of the separator by the doctor blade method, and the mass

loading of the KB/Mo₂C layer on the separator is about 0.6 mg cm⁻². The cross-section image of the KB/Mo₂C-modified separator shows the coating with about 25 μm in thickness (Fig. 1f). The elemental mappings of C and Mo element for the cross-section are shown in Fig. S3. The KB/Mo₂C-modified separator shows good mechanical stability without any exfoliation of the composites even when it is wrinkled, bent or soaked in the electrolyte (Fig. S4).

The visualized adsorption tests were carried out to evaluate the chemical adsorption between the Li₂S₆ and the Mo₂C. The KB/Mo₂C and KB with the same weight were immersed into the Li₂S₆ solution, respectively. As shown in Fig. 2a, the colour of the solution with only KB shows a slight change compared with the pristine Li₂S₆ solution, while the solution containing KB/Mo₂C is almost colourless. It is confirmed that although the specific surface area of KB/Mo₂C decreases, the Mo₂C provides plenty of adsorption site to immobilize the LiPSs. To further reveal the intrinsic affinity between LiPSs and Mo₂C, XPS testing of KB/Mo₂C before and after LiPSs adsorption was employed, as shown in Fig. 2b-c. The KB/Mo₂C immersed in the Li₂S₆ solution reveals S 2p signals at around 162.0 eV as shown in Fig. 2b. The Mo 3d spectrum of pristine KB/Mo₂C in Fig. 2c (top) shows the characteristic peaks of Mo 3d_{5/2} and 3d_{3/2}. The two peaks at 228.9 and 231.9 eV are ascribed to Mo²⁺ 3d_{5/2} and 3d_{3/2} in the carbide phase, respectively. The other peaks at 230.4 eV and 232.0 eV are attributed to Mo⁴⁺ and Mo⁶⁺ 3d_{5/2}, which is associated with the molybdenum oxide on Mo₂C surface [30]. After Li₂S₆ adsorption, the sulfur signal at 227.4 eV for S 2s is distinct [31], and the new peak corresponding to Mo-S at 229.1 eV [32] indicates strong affinity between Mo₂C and LiPSs. In S 2p spectrum, the peaks at 163.0 eV and 164.2 eV correspond to the S 2p_{3/2} and 2p_{1/2} for S⁻¹_T, and the peak at 163.6 eV attributes to the S 2p_{3/2} for S⁰_B (Fig. 2d). The peak at 167.5 eV is attributed to thiosulfate species [33]. As demonstrated by the visualized absorption test and XPS characterization, the “sulfiphilic” surface of Mo₂C can significantly retain the dissolved LiPSs in the cathode region and inhibit their diffusion through the separator to the Li anode.

To investigate the catalysis effect of Mo₂C on liquid LiPSs conversion, the symmetric cells with different electrodes (KB or KB/Mo₂C) in Li₂S₆

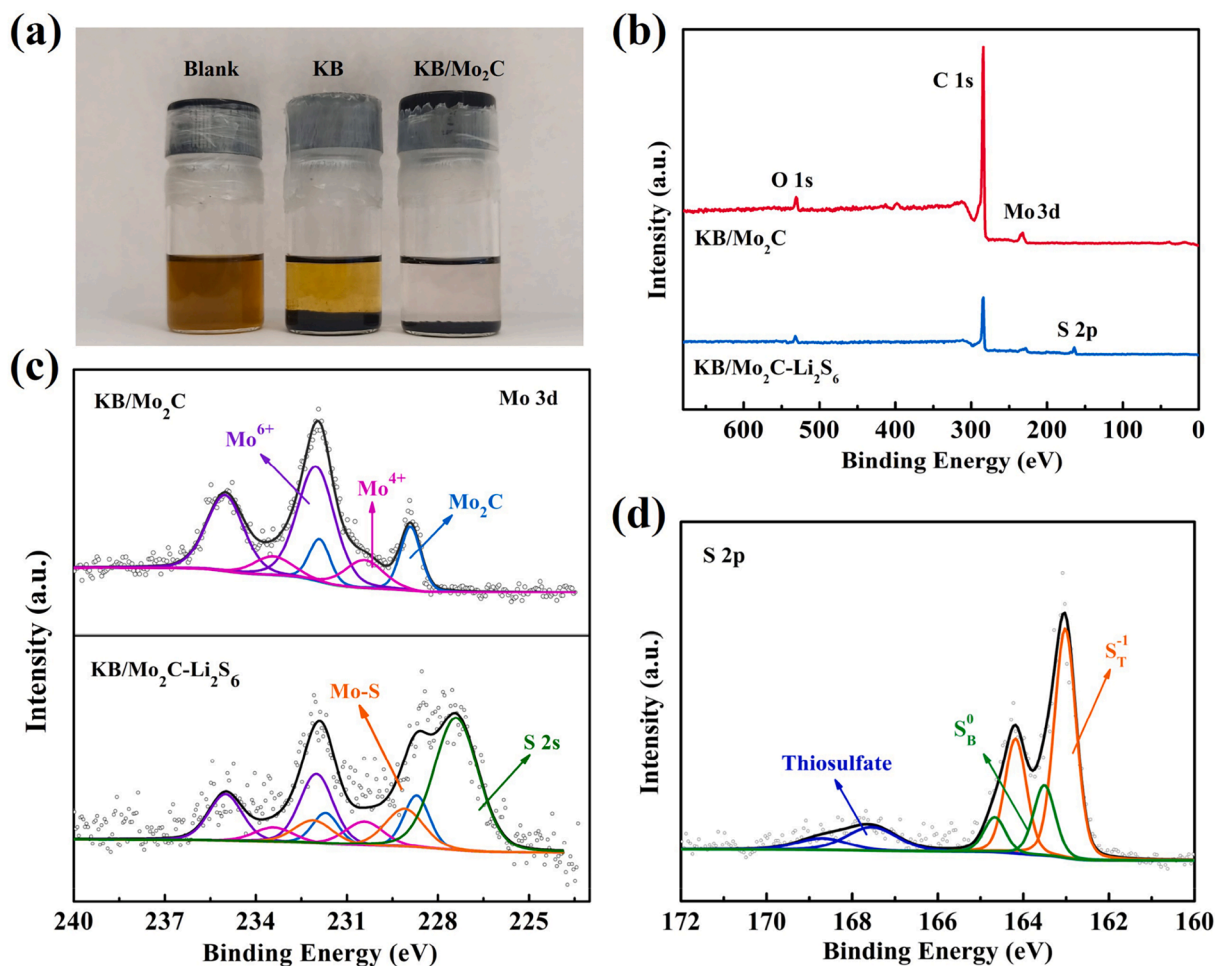


Fig. 2. (a) Photograph of the Li_2S_6 adsorption test. (b-d) XPS analysis of metal carbides before and after the adsorption test. (b) Wide-scan XPS spectra, (c) Mo 3d spectra and (d) S 2p spectrum.

electrolyte were assembled. Cyclic voltammetry (CV) testing was carried out within the voltage range of -0.8 to 0.8 V at a sweep rate of 20 mV s^{-1} . As shown in Fig. 3a, the polarization current of the symmetric cell based on the KB/ Mo_2C electrode shows a significant increase with two pairs of redox peaks. On the other hand, there is no obvious current response in the KB- Li_2S_6 system or the KB/ Mo_2C electrodes in the conventional electrolyte without Li_2S_6 . Furthermore, CV tests at different sweep rates were performed. The current peaks still present at lower sweep rates and augment with increasing sweep rates (Fig. S5a). The equation (1) is usually used to characterize the kinetics data, where i is the measured peak current and ν is the sweep rate.

$$i = a\nu^b \quad (1)$$

The measured peak current follows a power-law relationship with the sweep rate ν . The b value can be derived from the slope of the plot of $\log i$ vs. $\log \nu$. The b -values of 0.5 and 1 are two well-defined conditions. In particular, $b = 1$ indicates a capacitive behavior via a surface-controlled process, whereas $b = 0.5$ implies a reaction controlled by semi-infinite linear diffusion [34]. As shown in Fig. S5b, the plot of $\log i$ vs. $\log \nu$ demonstrates a good linear relationship, and the calculated b value is 0.44 for cathodic current peaks, indicating that the current response is derived from the redox of the Li_2S_6 . It demonstrates that the Mo_2C can not only trap the LiPSs, but also improve the reaction kinetics of LiPSs. Fig. 3b presents the chronoamperometry curves of the symmetrical cells at an overpotential of 250 mV. There is almost no current response on the KB electrode surface or the cell without Li_2S_6 active material, while the KB/ Mo_2C electrode shows much higher current

response (3 mA). This further implies that the redox reactions dominate the current responses instead of double-layer capacitance [35]. This high current response is mainly attributable to the synergy of adsorption, conductivity, and catalysis for LiPSs on Mo_2C surface.

To investigate the electrochemical reactions that occurred on the electrode, the symmetrical cells with KB/ Mo_2C electrode was disassembled during the CV test to analyze the cycled electrolyte on electrode surface. Fig. 3c shows the UV-visible absorption spectra of electrolyte samples at different stages during the CV scan. In the original solution, the strong absorption at around 270–280 nm is considered to be the Li_2S_6 [36]. After the occurrence of the first cathodic peak, the absorption signal of the Li_2S_6 decreases noticeably, indicating the consumption of the Li_2S_6 . After the second cathode peak, the signal of the Li_2S_6 further decreases, while a new absorption peak at 310 nm appears, corresponding to the S_3^{2-} species [36]. It demonstrates that Li_2S_6 is smoothly reduced to short-chain sulfides species on the KB/ Mo_2C surface. Electrochemical impedance spectra (EIS) were carried out to analyze the charge transfer resistance (R_{ct}) at the electrode/electrolyte interfaces. The Nyquist plots of the symmetrical cells are shown in Fig. 3d. It is shown that the KB/ Mo_2C electrode system exhibits a much smaller R_{ct} than the bare KB electrode, suggesting the accelerated electron transfer and reaction kinetics of Li_2S_6 in the KB/ Mo_2C electrode/electrolyte interphase.

The catalytic effect of Mo_2C on the LiPSs conversion in real Li-S cells is also investigated. The cells were assembled with different working electrode (KB, KB/ Mo_2C), lithium counter/reference electrode and Li_2S_6 electrolyte. CV curves at different sweep rates are shown in Fig. S6. Two

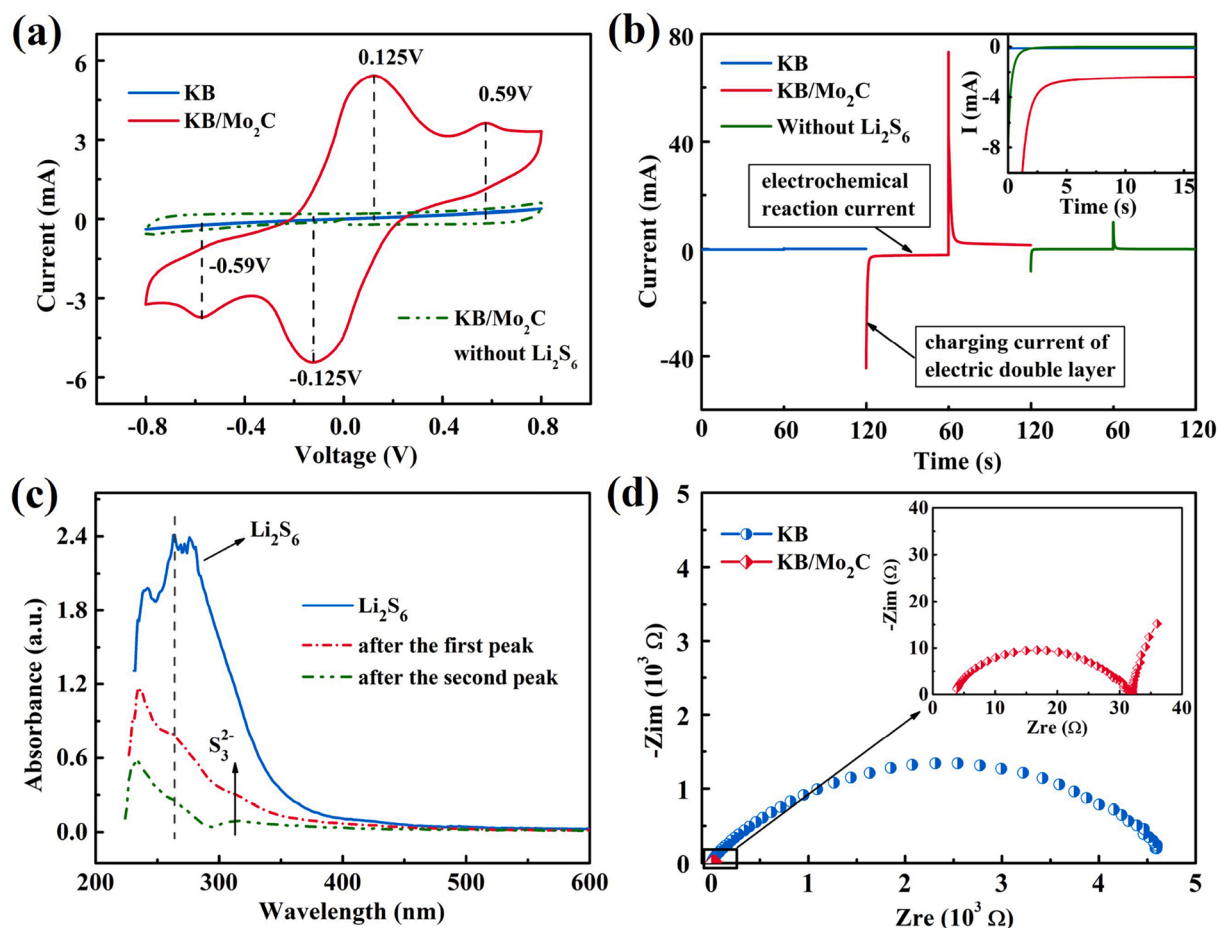


Fig. 3. (a) CV curves and (b) chronoamperometry curves of the symmetric cell with and without Li₂S₆. (c) UV-visible absorption spectra of electrolyte samples on the electrode at different stage. (d) EIS spectra of the symmetric cell.

distinct peaks during the cathodic process represent the conversion of Li₂S₆ to short-chain LiPSs and the further reduction to solid Li₂S₂/Li₂S, respectively. The anodic peak corresponds to the oxidation process of Li₂S/Li₂S₂ to sulfur [37]. It can be seen that the polarization increases on the KB electrode with the increasing sweep speed, whereas the redox potentials corresponding to the LiPSs conversion shifts slightly in the KB/Mo₂C system under the scanning. Meanwhile, the R_{ct} of the LiPSs conversion on the KB/Mo₂C electrode interface reduces compared with the KB electrode (Fig. S6c). The higher reaction currents and the smaller polarization indicate an easier conversion of LiPSs in the KB/Mo₂C system. The charging process of the cell is equally important. It is well known that the Li₂S suffers from sluggish kinetics, leading to a high overpotential at the initial charging [38]. The cells with Li₂S electrode and different separators were assembled to investigate the catalysis effect of Mo₂C on Li₂S activation. The conventional Li₂S electrode exhibits a high potential barrier at about 3.64 V (Fig. S7), indicating a sluggish activation process. However, the cell with the KB/Mo₂C-modified separator shows a lower potential barrier of 2.7 V, revealing kinetic promotion for the oxidation of Li₂S on the Mo₂C surface. It can be concluded that the Mo₂C is an excellent catalyst that can provide active sites for the LiPSs reduction and the Li₂S oxidation.

The Mo₂C exhibits strong chemical adsorption and catalysis for the LiPSs, which is expected to inhibit the shuttle effect and improve the cycling performance. To directly explore the effect of Mo₂C on electrochemical performance, Li-S cells with KB/Mo₂C-modified separator, KB-modified separator and bare PP separator were assembled. The sulfur host employs a kind of dual-shell carbon (DC) material, which is synthesized by a one-pot sol-gel process and subsequent carbonization process. The DC, with an average diameter of 230 nm (Fig. 4a and

Fig. S8a) and a large specific surface area of 708 m² g⁻¹ (Fig. S9), provides a physical barrier for the LiPSs and guarantees a high electronic conductivity. The DC/S composites maintain spheroidal morphology without agglomeration (Fig. 4c) and exhibit uniform distribution of sulfur (Fig. 4d-e). A sulfur content of 76 wt% in the DC/S composite was determined by thermal gravimetric analysis (Fig. S11). The CV tests were performed between 1.5 and 3.0 V at a scan rate of 0.1 mV s⁻¹. As shown in Fig. S12, two distinct peaks at around 2.25 V (Peak I) and 1.95 V (Peak II) during the cathodic scanning process represent the reduction of sulfur to high-order LiPSs (Li₂S₆/Li₂S₄) and the formation of solid-phase Li₂S₂/Li₂S, respectively. During the anodic scanning process, there exists one anodic peak at around 2.45 V (Peak III), which represents the oxidation process of Li₂S/Li₂S₂ to sulfur [39]. It is noteworthy that the cell with a KB/Mo₂C separator shows earlier onset potentials for redox reaction peaks, suggesting a decreased polarization and accelerated kinetics for the LiPSs conversion. Furthermore, CV tests under different sweep rates were performed to study the lithium ion diffusion coefficient. From the CV curves at different sweep rates (Fig. S13), the lithium ion diffusion coefficient can be calculated with the equation:

$$I_p = (2.69 \times 10^5) n^{1.5} S D_{Li^+}^{0.5} C_{Li} \nu^{0.5} \quad (2)$$

Where I_p is the peak current, S is the geometric area of the active electrode, n is the charge transfer number, D_{Li^+} is the lithium ion diffusion coefficient, C_{Li} is the concentration of lithium ions in cathode, and ν is the sweep rate [40]. The cathodic and anodic peak currents have a linear relationship with the square root of scanning rates (Fig. S13c-d). The slope value of the curve ($I_p/\nu^{0.5}$) represents the diffusion rate of lithium ions. The higher slope value in the cell with the KB/Mo₂C-

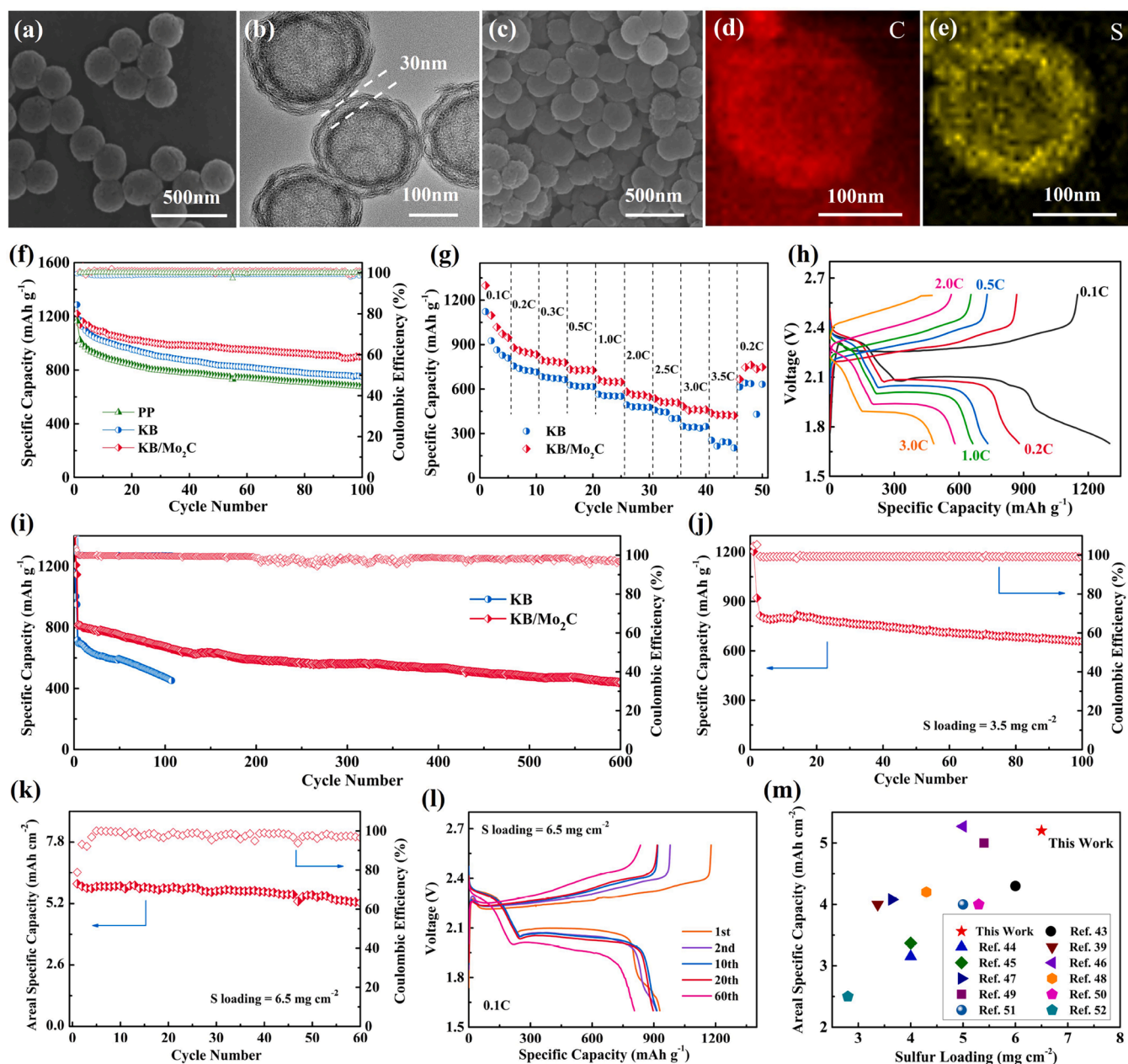


Fig. 4. (a) SEM and (b) TEM image of the as-synthesized DCs. (c) SEM image of the DC/S and the elemental mappings of (d) C, (e) S. Electrochemical performance of Li-S batteries with typical separator, KB-modified and KB/Mo₂C-modified separators: (f) Cycle performance at 0.2C; (g) Rate performance and (h) the corresponding galvanostatic discharge–charge profiles at different current densities; (i) Long cycling performance at a current density of 1C. (j) Cycling performance of Li-S battery with KB/Mo₂C-modified separator at 0.2C with a S loading of 3.5 mg cm⁻². (k) Cycling performance of Li-S battery with KB/Mo₂C-modified separator at 0.1C with a high S loading of 6.5 mg cm⁻² and (l) the corresponding discharge–charge curves. (m) Comparison of areal energy densities with other references.

modified separator demonstrates faster diffusion of lithium ions compared with the system based on the KB-modified separator. The fast transfer of electrons and lithium ions on the Mo₂C surface are favorable for the acceleration of the LiPSs redox reactions.

Li-S batteries with the KB/Mo₂C-modified separator exhibit improved electrochemical performance owing to obvious kinetic acceleration in the LiPSs conversion. It delivers an initial discharge capacity of 1221 mAh g⁻¹ at 0.2C and remaining 898 mAh g⁻¹ after 100 cycles with a capacity retention of 74% (Fig. 4f), which is higher than those with pristine PP (58%) and KB-modified PP (58%) separators. The rate performance of the cell was evaluated at increasing current rates from 0.1 to 3.5C (Fig. 4g). It can be observed that the cell using the KB/Mo₂C-modified separator shows specific capacities of 1299, 879, 796, 733, 664, 581, 536, 483, and 437 mAh g⁻¹ at 0.1, 0.2, 0.3, 0.5, 1, 2, 2.5, 3,

and 3.5C, respectively. After recovering the rate to 0.2C, a reversible capacity of 762 mAh g⁻¹ still can be achieved, suggesting the excellent reversibility at different rates. However, the cell using KB-modified separator only delivers discharge capacities of 1123, 756, 684, 627, 564, 494, 458, 349 and 256 mAh g⁻¹ at corresponding discharge rate. Fig. 4h shows the corresponding charge/discharge curves at varied current rates. There exist two discharge platforms and one charge platform corresponding to the redox peaks in CV curves. Although the voltage polarization increases with the increasing current density, there still exist two obvious discharge plateaus even at 3.5C.

In addition, the cell with KB/Mo₂C-modified separator exhibits a high active material utilization and Coulombic efficiency at 0.5C even in LiNO₃-free electrolyte (Fig. S14). Generally, the shuttle effect can be suppressed in the electrolyte with LiNO₃ additive by passivating lithium

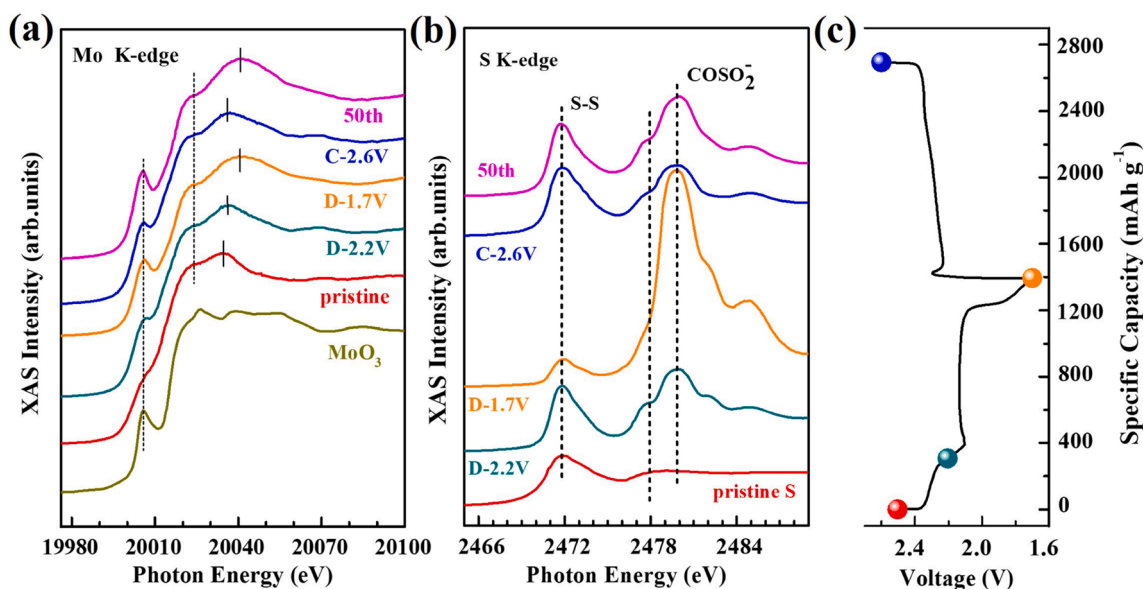


Fig. 5. Ex-situ XANES of (a) Mo K-edge and (b) S K-edge for the separator at certain states of charge/discharge during the first cycle and after 50 cycles. (c) The corresponding discharge-charge curves.

metal surface and it becomes aggravated in the LiNO_3 -free electrolyte [41]. The high Coulombic efficiency of the battery with LiNO_3 -free electrolyte and modified separator demonstrates that the shuttle effect is effectively suppressed by the KB/ Mo_2C layer. The long cycling stabilities of the cells at 1C are shown in Fig. 4i. The cell with the KB/ Mo_2C -modified separator exhibits an initial reversible discharge capacity of 813 mAh g^{-1} at 1C after three-cycle activation at 0.1C, and it still retains reversible capacity of 439 mAh g^{-1} after 600 cycles with a low capacity decay of 0.076% per cycle, demonstrating outstanding cycling stability. However, the cell using KB-modified separator only delivers 716 mAh g^{-1} at 1C and the discharge capacity rapidly decays to 464 mAh g^{-1} after 100 cycles. The improved cycling stability and rate performance are resulted from the multifunctional modified separator which can anchor and catalyze the LiPSs. Meanwhile, the effect of Mo_2C amount on performance was also investigated. Increasing the Mo_2C amount to 50%, the cell shows reduced specific capacity and lower capacity retention of 64% at 0.2C (Fig. S15). The increasing Mo_2C may cause the agglomeration of materials, thus reducing the catalytic active surface area, and leading to a low utilization of active material.

It is very important to attain the practical high energy-density of Li-S batteries by adopting high areal loading electrodes. Therefore, the cathode with a high sulfur loading of 3.5 and 6.5 mg cm^{-2} were further prepared. The cathode with 3.5 mg cm^{-2} loading shows a remarkable discharge capacity of 812 mAh g^{-1} at 0.2C and high capacity retention of 81% after 100 cycles (Fig. 4j). When the sulfur loading increases to 6.5 mg cm^{-2} , the cell with the KB/ Mo_2C -modified separator delivers a specific capacity of 929 mAh g^{-1} at 0.1C and a remarkable capacity retention of 805 mAh g^{-1} (corresponding to an areal specific capacity of 5.2 mAh cm^{-2}) after 60 cycles (Fig. 4k). The charge/discharge curves (Fig. 4l) exhibit typical two discharge platforms and one charging platform, corresponding to the CV curves. The Coulombic efficiency in the first cycle is a little lower than those in the following cycles. In high sulfur loading cathode, plenty of LiPSs form during the discharging/charging process. The self-discharge and the shuttle effect will cause the over charge of Li-S batteries [42]. Some Mo_2C inside the modified layer may be constantly activated during cycling, and the increased utilization of Mo_2C will accelerate the conversion efficiency of LiPSs, effectively suppressing the shuttle effect of LiPSs. Therefore, the Coulombic efficiency of the lithium sulfur battery increases in the following cycles. The excellent capacity of high-loading electrode is higher than those in the reported works [39,43–52], as shown in Fig. 4m. The KB/ Mo_2C -

modified separator plays an important role on intercepting, anchoring and catalyzing LiPSs to inhibit the shuttling effect in Li-S battery. Therefore, the cells based on the KB/ Mo_2C -modified separator demonstrate higher Coulombic efficiency, improved rate capability and excellent cycling stability. Furthermore, the cell with a high sulfur loading of 6.5 mg cm^{-2} exerted a high areal specific capacity and excellent cycling stability.

To verify the general applicability of KB/ Mo_2C -modified separator in Li-S batteries, the cells combining KB/S cathode and modified separators were assembled. As shown in Fig. S16, the cell using KB/S cathode and KB/ Mo_2C -modified separator exhibits a specific capacity of 678 mAh g^{-1} after 100 cycles with a capacity retention of 60%. It is indicated that the incorporation of Mo_2C catalyst in the modified separator is beneficial to improve the utilization of active material. Furthermore, the electrochemical performance of sulfur cathode with the KB/ Mo_2C as host material was evaluated. The XRD pattern of the KB/ Mo_2C /S shows obvious diffraction peaks of sulfur and Mo_2C as shown in Fig. S17a. The sulfur content of 73.5% in composites is confirmed according to the TGA curves (Fig. S17b). The KB/S/ Mo_2C cathode delivers an initial discharge capacity of 921 mAh g^{-1} at 0.2C, remaining 659 mAh g^{-1} after 100 cycles with a high Coulombic efficiency of 99% (Fig. S18a). However, the KB/S cathode exhibits low active material utilization and its Coulombic efficiency reduces to 96% during cycling. The KB/ Mo_2C /S cathodes with the increased sulfur loading to 4.8 mg cm^{-2} can still deliver a high discharge capacity of 889 mAh g^{-1} at 0.1C as shown in Fig. S18b. After 70 cycles, it remains a specific capacity of 761 mAh g^{-1} with a capacity retention of 86%. The improved specific capacity and Coulomb efficiency is derived from the efficient adsorption and catalytic conversion of LiPSs on Mo_2C .

X-ray absorption near edge structure (XANES) was further conducted to illuminate the reaction mechanism of Mo_2C and LiPS during the charge/discharge process. Fig. 5a shows the Mo K-edge spectra at different charge/discharge states. The Mo K-edge of the pristine KB/ Mo_2C exhibits two peaks at 20022 eV and 20035 eV [53]. The peak at 20035 eV shifts to higher energy and shows a higher intensity during discharge process, which may be caused by the strong affinity between LiPSs and Mo to partially form Mo-S bond on the Mo_2C surface [54,55]. In addition, the pre-edge peak at about 20005 eV corresponds to the Mo^{6+} structure [56], indicating that the electron transfers from Mo to LiPSs. The peak at 20035 eV shifts back partially after the cell is charged to 2.6 V, and then changes to a higher energy after 50 cycles, which

suggests that a stable C-Mo-S bonding may form on the Mo₂C surface. The S K-edge at different states of charge/discharge is shown in Fig. 5b. For the S K-edge, the peak at 2471.9 eV and 2479.8 eV can be attributed to the S-S bond in elemental S and the COSO₂⁻ in LiTFSI [57]. The intensity of the S-S bond decreases in the discharge process, which represents the reduction of the S₈. The peak at 2478 eV corresponding to S²⁻ in sulfide appears and becomes stable after 50 cycles [55,58], demonstrating strong interaction between Mo and S. In conclusion, the electron transfer occurs between Mo and S during the charge/discharge process, and stable C-Mo-S bonding may form on the Mo₂C surface after several cycles owing to the strong affinity between Mo₂C and LiPSs.

4. Conclusion

In summary, we demonstrate a KB/Mo₂C-modified separator for high-performance Li-S batteries. The KB/Mo₂C is prepared by depositing Mo₂C particles on KB through a simple carburization method. The Mo₂C nanoparticle as adsorption and catalytic sites trap the dissolved LiPSs and accelerate the reaction kinetics of LiPSs conversion, improving the utilization of sulfur and suppressing the shuttling effect. The Li-S batteries with the KB/Mo₂C-modified separator exhibit high sulfur utilization and excellent electrochemical performance. Outstanding cycling stability at a relatively high rate of 1C with a low capacity decay rate of 0.076% per cycle is achieved in the tested Li-S batteries. The cathode, with a high sulfur loading of 6.5 mg cm⁻², shows a high areal specific capacity of 5.2 mAh cm⁻² after 60 cycles at a current rate of 0.1C. The multifunctional modified separator, combining the intercepting/anchoring LiPSs and catalyzing LiPSs conversion, is an effective strategy to improve the electrochemical performance of Li-S batteries.

Declaration of Competing Interest

The authors declare that they have no known competing financial interests or personal relationships that could have appeared to influence the work reported in this paper.

Acknowledgments

This research was supported by the National Natural Science Foundation of China (no. 51772068), Natural Sciences and Engineering Research Council of Canada (NSERC), Canada Research Chair Program (CRC), Canada Foundation for Innovation (CFI), Ontario Research Fund, the Canada Light Source at University of Saskatchewan (CLS), Interdisciplinary Development Initiatives (IDI) by Western University, and University of Western Ontario.

Appendix A. Supplementary data

Supplementary data to this article can be found online at <https://doi.org/10.1016/j.cej.2021.128563>.

References

- J. Lu, Z. Chen, Z. Ma, F. Pan, L.A. Curtiss, K. Amine, The role of nanotechnology in the development of battery materials for electric vehicles, *Nature Nanotech* 11 (2016) 1031–1038.
- M.M. Thackeray, C. Wolverton, E.D. Isaacs, Electrical energy storage for transportation—approaching the limits of and going beyond lithium-ion batteries, *Energy Environ. Sci.* 5 (2012) 7854.
- X. Li, M. Banis, A. Lushington, X. Yang, Q. Sun, Y. Zhao, C. Liu, Q. Li, B. Wang, W. Xiao, C. Wang, M. Li, J. Liang, R. Li, Y. Hu, L. Goncharova, H. Zhang, T.K. Sham, X. Sun, A high-energy sulfur cathode in carbonate electrolyte by eliminating polysulfides via solid-phase lithium-sulfur transformation, *Nat. Commun.* 9 (2018) 4509.
- X. Yang, X. Li, K. Adair, H. Zhang, X. Sun, Structural Design of Lithium-Sulfur Batteries: From Fundamental Research to Practical Application, *Electrochem. Energy Rev.* 1 (2018) 239–293.
- J.-G. Wang, K. Xie, B. Wei, Advanced engineering of nanostructured carbons for lithium-sulfur batteries, *Nano Energy* 15 (2015) 413–444.
- T. Tang, Y. Hou, Multifunctionality of Carbon-based Frameworks in Lithium Sulfur Batteries, *Electrochem. Energy Rev.* 1 (2018) 403–432.
- C.-Y. Fan, Y.-P. Zheng, X.-H. Zhang, Y.-H. Shi, S.-Y. Liu, H.-C. Wang, X.-L. Wu, H.-Z. Sun, J.-P. Zhang, High-Performance and Low-Temperature Lithium-Sulfur Batteries: Synergism of Thermodynamic and Kinetic Regulation, *Adv. Energy Mater.* 8 (2018) 1703638.
- X. Ji, K.T. Lee, L.F. Nazar, A highly ordered nanostructured carbon-sulphur cathode for lithium-sulphur batteries, *Nature Mater.* 8 (2009) 500–506.
- P. Zuo, W. Zhang, J. Hua, Y. Ma, C. Du, X. Cheng, Y. Gao, G. Yin, A Novel One-dimensional Reduced Graphene Oxide/Sulfur Nanoscroll Material and its Application in Lithium Sulfur Batteries, *Electrochim. Acta* 222 (2016) 1861–1869.
- P. Zuo, H. Zhang, M. He, Q. Li, Y. Ma, C. Du, X. Cheng, H. Huo, Y. Gao, G. Yin, Clew-like N-doped multiwalled carbon nanotube aggregates derived from metal-organic complexes for lithium-sulfur batteries, *Carbon* 122 (2017) 635–642.
- C. Zhang, H.B. Wu, C. Yuan, Z. Guo, X.W.D. Lou, Confining Sulfur in Double-Shelled Hollow Carbon Spheres for Lithium-Sulfur Batteries, *Angew. Chem. Int. Ed.* 51 (2012) 9592–9595.
- G. Babu, K. Ababtain, K.Y. Ng, L.M. Arava, Electrocatalysis of lithium polysulfides: current collectors as electrodes in Li/S battery configuration, *Sci Rep* 5 (2015) 8763.
- P. Zuo, J. Hua, M. He, H. Zhang, Z. Qian, Y. Ma, C. Du, X. Cheng, Y. Gao, G. Yin, Facilitating the redox reaction of polysulfides by an electrocatalytic layer-modified separator for lithium-sulfur batteries, *J. Mater. Chem. A* 5 (2017) 10936–10945.
- Z. Yuan, H.-J. Peng, T.-Z. Hou, J.-Q. Huang, C.-M. Chen, D.-W. Wang, X.-B. Cheng, F. Wei, Q. Zhang, Powering Lithium-Sulfur Battery Performance by Propelling Polysulfide Redox at Sulfiphilic Hosts, *Nano Lett.* 16 (2016) 519–527.
- Y. Tao, Y. Wei, Y. Liu, J. Wang, W. Qiao, L. Ling, D. Long, Kinetically-enhanced polysulfide redox reactions by Nb₂O₅ nanocrystals for high-rate lithium-sulfur battery, *Energy Environ. Sci.* 9 (2016) 3230–3239.
- D.-R. Deng, T.-H. An, Y.-J. Li, Q.-H. Wu, M.-S. Zheng, Q.-F. Dong, Hollow porous titanium nitride tubes as a cathode electrode for extremely stable Li-S batteries, *J. Mater. Chem. A* 4 (2016) 16184–16190.
- K. Xiao, J. Wang, Z. Chen, Y. Qian, Z. Liu, L. Zhang, X. Chen, J. Liu, X. Fan, Z. X. Shen, Improving Polysulfides Adsorption and Redox Kinetics by the Co₃N Nanoparticle/N-Doped Carbon Composites for Lithium-Sulfur Batteries, *Small* 15 (2019), e1901454.
- Y. Zhong, L. Yin, P. He, W. Liu, Z. Wu, H. Wang, Surface Chemistry in Cobalt Phosphide-Stabilized Lithium-Sulfur Batteries, *J. Am. Chem. Soc.* 140 (2018) 1455–1459.
- K. Xiao, Z. Chen, Z. Liu, L. Zhang, X. Cai, C. Song, Z. Fan, X. Chen, J. Liu, Z.X. Shen, N-doped carbon sheets arrays embedded with CoP nanoparticles as high-performance cathode for Li-S batteries via triple synergistic effects, *J. Power Sources* 455 (2020), 227959.
- H.-J. Peng, G.-e. Zhang, X. Chen, Z.-W. Zhang, W.-T. Xu, J.-Q. Huang, Q. Zhang, Enhanced Electrochemical Kinetics on Conductive Polar Mediators for Lithium-Sulfur Batteries, *Angew. Chem. Int. Ed.* 55 (2016) 12990–12995.
- B. Yu, D. Chen, Z. Wang, F. Qi, X. Zhang, X. Wang, Y. Hu, B. Wang, W. Zhang, Y. Chen, J. He, W. He, Mo₂C quantum dots@graphene functionalized separator toward high-current-density lithium metal anodes for ultrastable Li-S batteries, *Chem. Eng. J.* 399 (2020), 125837.
- Z. Wang, J. Liu, L. Sun, Y. Zhang, Q. Fu, H. Xie, H. Sun, Porous Molybdenum Carbide Nanorods as Novel “Bifunctional” Cathode Material for Li-S Batteries, *Chem. Eur. J.* 24 (2018) 14154–14161.
- C. Shang, L. Cao, M. Yang, Z. Wang, M. Li, G. Zhou, X. Wang, Z. Lu, Freestanding Mo₂C-decorating N-doped carbon nanofibers as 3D current collector for ultra-stable Li-S batteries, *Energy Storage Mater.* 18 (2019) 375–381.
- R. Razaq, N. Zhang, Y. Xin, Q. Li, J. Wang, Z. Zhang, Electrocatalytic conversion of lithium polysulfides by highly dispersed ultrafine Mo₂C nanoparticles on hollow N-doped carbon flowers for Li-S batteries, *EcoMat* 2 (2020).
- R. Razaq, D. Sun, Y. Xin, Q. Li, T. Huang, L. Zheng, Z. Zhang, Y. Huang, Enhanced kinetics of polysulfide redox reactions on Mo₂C/CNT in lithium-sulfur batteries, *Nanotechnology* 29 (2018), 295401.
- G. Zhou, S. Pei, L. Li, D.-W. Wang, S. Wang, K. Huang, L.-C. Yin, F. Li, H.-M. Cheng, A Graphene-Pure-Sulfur Sandwich Structure for Ultrafast, Long-Life Lithium-Sulfur Batteries, *Adv. Mater.* 26 (2014) 625–631.
- I. Bauer, S. Thieme, J. Brückner, H. Althues, S. Kaskel, Reduced polysulfide shuttle in lithium-sulfur batteries using Nafion-based separators, *J. Power Sources* 251 (2014) 417–422.
- S.-H. Chung, A. Manthiram, High-Performance Li-S Batteries with an Ultra-lightweight MWCNT-Coated Separator, *J. Phys. Chem. Lett.* 5 (2014) 1978–1983.
- L. Fan, M. Li, X. Li, W. Xiao, Z. Chen, J. Lu, Interlayer Material Selection for Lithium-Sulfur Batteries, *Joule* 3 (2019) 361–386.
- C. Lv, J. Wang, Q. Huang, Q. Yang, Z. Huang, C. Zhang, Facile synthesis of hollow carbon microspheres embedded with molybdenum carbide nanoparticles as an efficient electrocatalyst for hydrogen generation, *RSC Adv.* 6 (2016) 75870–75874.
- M.R. Islam, N. Kang, U. Bhanu, H.P. Paudel, M. Eremtchouk, L. Tetard, M. N. Leuenberger, S.I. Khondaker, Tuning the electrical property via defect engineering of single layer MoS₂ by oxygen plasma, *Nanoscale* 6 (2014) 10033–10039.
- F. Zhou, Z. Li, X. Luo, T. Wu, B. Jiang, L.-L. Lu, H.-B. Yao, M. Antonietti, S.-H. Yu, Low Cost Metal Carbide Nanocrystals as Binding and Electrocatalytic Sites for High Performance Li-S Batteries, *Nano Lett.* 18 (2018) 1035–1043.
- Q. Pang, D. Kundu, M. Cuisinier, L.F. Nazar, Surface-enhanced redox chemistry of polysulfides on a metallic and polar host for lithium-sulphur batteries, *Nat. Commun.* 5 (2014) 4759.

- [34] V. Augustyn, J. Come, M.A. Lowe, J.W. Kim, P.-L. Taberna, S.H. Tolbert, H. D. Abruña, P. Simon, B. Dunn, High-rate electrochemical energy storage through Li^+ intercalation pseudocapacitance, *Nature Mater* 12 (2013) 518–522.
- [35] J. Pu, Z. Shen, J. Zheng, W. Wu, C. Zhu, Q. Zhou, H. Zhang, F. Pan, Multifunctional Co_3S_4 @sulfur nanotubes for enhanced lithium-sulfur battery performance, *Nano Energy* 37 (2017) 7–14.
- [36] C. Barchasz, F. Molton, C. Duboc, J.C. Lepretre, S. Patoux, F. Alloin, Lithium/sulfur cell discharge mechanism: an original approach for intermediate species identification, *Anal. Chem.* 84 (2012) 3973–3980.
- [37] H. Xu, L. Qie, A. Manthiram, An integrally-designed, flexible polysulfide host for high-performance lithium-sulfur batteries with stabilized lithium-metal anode, *Nano Energy* 26 (2016) 224–232.
- [38] B.L. Mehdi, A. Stevens, J. Qian, C. Park, W. Xu, W.A. Henderson, J.G. Zhang, K. T. Mueller, N.D. Browning, The Impact of Li Grain Size on Coulombic Efficiency in Li Batteries, *Sci Rep* 6 (2016) 34267.
- [39] J. Zhu, Y. Ge, D. Kim, Y. Lu, C. Chen, M. Jiang, X. Zhang, A novel separator coated by carbon for achieving exceptional high performance lithium-sulfur batteries, *Nano Energy* 20 (2016) 176–184.
- [40] G. Zhou, H. Tian, Y. Jin, X. Tao, B. Liu, R. Zhang, Z.W. Seh, D. Zhuo, Y. Liu, J. Sun, J. Zhao, C. Zu, D.S. Wu, Q. Zhang, Y. Cui, Catalytic oxidation of Li_2S on the surface of metal sulfides for Li-S batteries, *Proc. Natl. Acad. Sci. USA* 114 (2017) 840–845.
- [41] M. Barghamadi, A.S. Best, A.I. Bhatt, A.F. Hollenkamp, P.J. Mahon, M. Musameh, T. Rütther, Effect of LiNO_3 additive and pyrrolidinium ionic liquid on the solid electrolyte interphase in the lithium-sulfur battery, *J. Power Sources* 295 (2015) 212–220.
- [42] S. Xiong, K. Xie, Y. Diao, X. Hong, Properties of surface film on lithium anode with LiNO_3 as lithium salt in electrolyte solution for lithium-sulfur batteries, *Electrochim. Acta* 83 (2012) 78–86.
- [43] L. Zhang, X. Chen, F. Wan, Z. Niu, Y. Wang, Q. Zhang, J. Chen, Enhanced Electrochemical Kinetics and Polysulfide Traps of Indium Nitride for Highly Stable Lithium-Sulfur Batteries, *ACS Nano* 12 (2018) 9578–9586.
- [44] Z. Li, L. Tang, X. Liu, T. Song, Q. Xu, H. Liu, Y. Wang, A polar TiO/MWCNT coating on a separator significantly suppress the shuttle effect in a lithium-sulfur battery, *Electrochim. Acta* 310 (2019) 1–12.
- [45] P. Han, A. Manthiram, Boron- and nitrogen-doped reduced graphene oxide coated separators for high-performance Li-S batteries, *J. Power Sources* 369 (2017) 87–94.
- [46] S. Wang, X. Qian, L. Jin, D. Rao, S. Yao, X. Shen, K. Xiao, S. Qin, Separator modified by Y_2O_3 nanoparticles-Ketjen Black hybrid and its application in lithium-sulfur battery, *J Solid State Electrochem* 21 (2017) 3229–3236.
- [47] L. Tan, X. Li, Z. Wang, H. Guo, J. Wang, Lightweight Reduced Graphene Oxide@ MoS_2 Interlayer as Polysulfide Barrier for High-Performance Lithium-Sulfur Batteries, *ACS Appl. Mater. Interfaces* 10 (2018) 3707–3713.
- [48] Y.i. Guo, M. Sun, H. Liang, W. Ying, X. Zeng, Y. Ying, S. Zhou, C. Liang, Z. Lin, X. Peng, Blocking Polysulfides and Facilitating Lithium-Ion Transport: Polystyrene Sulfonate@HKUST-1 Membrane for Lithium-Sulfur Batteries, *ACS Appl. Mater. Interfaces* 10 (2018) 30451–30459.
- [49] J. Balach, H.K. Singh, S. Gomoll, T. Jaumann, M. Klose, S. Oswald, M. Richter, J. Eckert, L. Giebeler, Synergistically Enhanced Polysulfide Chemisorption Using a Flexible Hybrid Separator with N and S Dual-Doped Mesoporous Carbon Coating for Advanced Lithium-Sulfur Batteries, *ACS Appl. Mater. Interfaces* 8 (2016) 14586–14595.
- [50] H.J. Peng, D.W. Wang, J.Q. Huang, X.B. Cheng, Z. Yuan, F. Wei, Q. Zhang, Janus Separator of Polypropylene-Supported Cellular Graphene Framework for Sulfur Cathodes with High Utilization in Lithium-Sulfur Batteries, *Adv Sci (Weinh)* 3 (2016), 1500268.
- [51] C.-Y. Fan, H.-Y. Yuan, H.-H. Li, H.-F. Wang, W.-L. Li, H.-Z. Sun, X.-L. Wu, J.-P. Zhang, The Effective Design of a Polysulfide-Trapped Separator at the Molecular Level for High Energy Density Li-S Batteries, *ACS Appl. Mater. Interfaces* 8 (2016) 16108–16115.
- [52] J. Song, D. Su, X. Xie, X. Guo, W. Bao, G. Shao, G. Wang, Immobilizing Polysulfides with MXene-Functionalized Separators for Stable Lithium-Sulfur Batteries, *ACS Appl. Mater. Interfaces* 8 (2016) 29427–29433.
- [53] J.S. Lee, J.E. Yie, An XANES study of carbides of molybdenum and tungsten, *Korean J. Chem. Eng.* 8 (1991) 164–167.
- [54] Y. Kim, D.H.K. Jackson, D. Lee, M. Choi, T.-W. Kim, S.-Y. Jeong, H.-J. Chae, H. W. Kim, N. Park, H. Chang, T.F. Kuech, H.J. Kim, In Situ Electrochemical Activation of Atomic Layer Deposition Coated MoS_2 Basal Planes for Efficient Hydrogen Evolution Reaction, *Adv. Funct. Mater.* 27 (2017) 1701825.
- [55] L. Cai, J. He, Q. Liu, T. Yao, L. Chen, W. Yan, F. Hu, Y. Jiang, Y. Zhao, T. Hu, Z. Sun, S. Wei, Vacancy-induced ferromagnetism of MoS_2 nanosheets, *J. Am. Chem. Soc.* 137 (2015) 2622–2627.
- [56] U.K. Sen, P. Johari, S. Basu, C. Nayak, S. Mitra, An experimental and computational study to understand the lithium storage mechanism in molybdenum disulfide, *Nanoscale* 6 (2014) 10243–10254.
- [57] X. Li, A. Lushington, Q. Sun, W. Xiao, J. Liu, B. Wang, Y. Ye, K. Nie, Y. Hu, Q. Xiao, R. Li, J. Guo, T.-K. Sham, X. Sun, Safe and Durable High-Temperature Lithium-Sulfur Batteries via Molecular Layer Deposited Coating, *Nano Lett.* 16 (2016) 3545–3549.
- [58] V.R. Surisetty, Y. Hu, A.K. Dalai, J. Kozinski, Structural characterization and catalytic performance of alkali (K) and metal (Co and Rh)-promoted MoS_2 catalysts for higher alcohols synthesis, *Appl. Catal. A* 392 (2011) 166–172.